J. Fluid Mech. (2005), *vol.* 530, *pp.* 197–212. © 2005 Cambridge University Press
doi:10.1017/S0022112005003782 Printed in the United Kingdom

Translating circular thrust bearings

By ROBERT E. JOHNSON[1] AND NOAH D. MANRING[2]

[1]The William States Lee College of Engineering, University of North Carolina – Charlotte, Charlotte, NC 28223, USA

[2]Mechanical and Aerospace Engineering Department, University of Missouri – Columbia, Columbia, MO 65211, USA

(Received 23 February 2004 and in revised form 3 December 2004)

Thrust bearings have been the object of a considerable amount of research for many years. The attention that these bearings have received is primarily due to the important role they play in the design and operation of heavy equipment. The objectives of this work are to examine the effect of translation and bearing geometry, such as recess depth and width, on the performance of circular thrust bearings. A closed-form solution is obtained for laminar viscous flow that extends prior results which generally focus on stationary or hydrostatic bearings. Earlier studies have examined specific aspects of translation, such as recirculation in the recess, but the current study is a comprehensive analysis in the case of laminar flow. The analysis reveals a single dimensionless parameter that describes the influence of the bearing speed. Expressions that predict the load-carrying capacity of the bearing, the tilting moment exerted on the bearing, the volumetric leakage of the bearing, and power due to lubricant injection and translation are obtained. Streamline patterns under the bearing show conditions at higher speeds when the injected lubricant does not penetrate underneath the entire bearing surface.

1. Introduction

Circular thrust bearings have been used for many years to provide a mechanism for lubricating sliding surfaces. These bearings are lubricated primarily by using an external pump to inject fluid between the bearing and thrust surface. Thrust bearings are classically used in hydraulic machinery that is heavily loaded and operated at low speeds. Historically, most design work is based on the well-known results for stationary or hydrostatic thrust bearings. It is also popular to use deep recesses (or pockets) since these bearings are easy to analyse because the lands are often relatively small and the pressure beneath the bearing is essentially constant in the recess. Therefore, the load-carrying capacity of the bearing is easily estimated by multiplying the supplied pressure by the surface area of the bearing recess. Corrections for the pressure distribution on the land area can also be easily included to improve accuracy, if necessary.

The hydrostatic thrust bearing has received extensive attention in the literature and overviews can be found in many places, such as Bassani & Piccigallo (1992), Rowe (1983) or Szeri (1998). Hamrock (1994) is particularly useful for the design engineer since it presents analytical results for a wide variety of bearing configurations. Many studies focus on a stationary bearing having a deep recess and a pressure field induced by lubricant injection alone. They also generally neglect bearing translation and film squeezing. In some cases, estimates of translational effects are made to account

https://doi.org/10.1017/S0022112005003782 Published online by Cambridge University Press

for power consumed by the recirculating flow in the recess. For example, Shinkle & Hornung (1965) considered journal-bearing translation and calculated the total viscous drag due to the lands and recesses. Similarly, Bassani & Piccigallo (1992) considered the same problem of two-dimensional thrust bearings, but only accounted for the contribution from the recess. The effects of translation and squeezing are often referred to as hydrodynamic effects versus hydrostatic effects (although strictly speaking the pressures induced by bearing motion and lubricant injection are both hydrodynamic forces). In applications such as axial piston pumps, the bearing translates across a thrust surface and therefore it is relevant to examine the effect of translation. Here, we explore translating circular thrust bearings and the influence of various recess designs on bearing performance.

A wide range of other studies also exist and, although we make no attempt to review this vast literature, it is useful to give the reader a flavour of what is available. Variation in bearing geometry is often a central issue, such as the study by O'Donoghue & Hooke (1969) which examined tapered lands, stepped (recess) bearing and grooved lands. Other studies have analysed stationary bearings with shallow and tapered recesses (Rowe 1983; Bassani & Piccigallo 1992) and the inherent compensation of shallow and tapered recess bearing geometry has long been recognized. More recently, patent protection has been obtained for other concepts involving shallow recess designs (Ivantysyn 1999). Another frequently investigated geometric feature is the number and arrangement of recesses and lands or pads. This includes the experimental comparison of central recess versus multi-recess thrust bearings conducted by Osman *et al.* (1996) and the experiments on a rotating eight-pad thrust bearing using typical operating conditions by Dadouche, Fillon & Bligoud (2000). For a circular thrust bearing rotating about its symmetry axis, San Andrés (2000) conducted a numerical investigation of the fluid/thermal equations with four recesses positioned around the periphery of the bearing. A small-amplitude squeezing motion and inertial effects were included. Somewhat related to these multi-pad bearing studies are the studies of self-alignment of tilted two-dimensional multi-pad thrust bearings by van Beek & Ostayen (1997) which included the overall hydraulic network, and the numerical solutions for tilted thrust bearings of finite length by van Beek & Segal (1997). In addition to the various geometric features that might be designed into a bearing, the effect of bearing deformation has also attracted attention. Dowson & Taylor (1967) examined elasto-hydrostatic lubrication and Wang, Zhang & Zhang (1999) considered thermo-elastic hydrodynamic lubrication. In an attempt to capitalize on bearing deformation, Davies (1974) explored the novel concept of a flexible-plate thrust bearing to enhance performance. With the current application interest in axial piston pumps, note that Iboshi & Yamaguchi (1982) solved the coupled equations of bearing vertical motion and bearing pressure to evaluate axial pump performance. Subsequently, they examined the effect of surface roughness (Iboshi & Yamaguchi 1986). At the device level, Storteig & White (1999) were concerned about the influence of thrust bearings on shaft vibrations and Kazama & Yamaguchi (1993) focused on numerical optimization for design. Note that the majority of the modelling studies above have been numerical investigations. In addition to this, a wealth of online interactive tools is also available at www.tribology-abc.com for stationary bearings (see also van Beek 2004).

Though the existing body of literature on hydrostatic thrust bearings is vast, few studies have fully explored the effects of translation and recess geometry on performance. This work is aimed at addressing these questions for circular thrust bearings. The goal is to obtain simple expressions for engineering quantities useful in design. A

https://doi.org/10.1017/S0022112005003782 Published online by Cambridge University Press

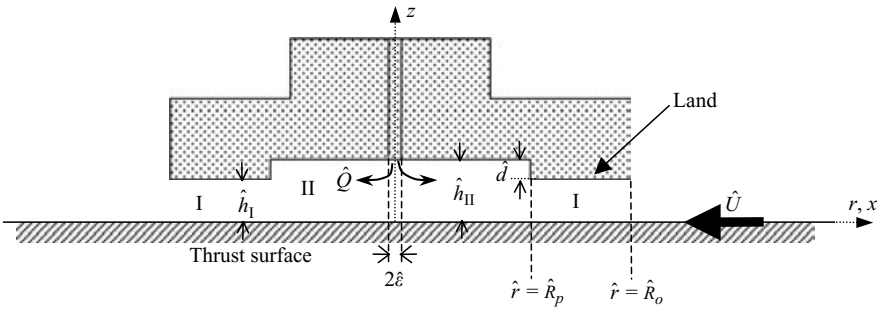


FIGURE 1. Circular thrust bearing geometry.

single dimensionless parameter is found to describe the influence of the bearing speed under laminar flow conditions. The principal results include closed-form expressions describing the load-carrying capacity of the bearing, the tilting moment, the volumetric leakage (or efficiency) of the bearing and power consumed by lubricant injection and translation (i.e. drag). Flow patterns under the bearing surface are also presented and indicate that high-speed bearings operating in an unflooded environment have the potential to operate partially dry. The results are discussed and conclusions are summarized in the final section of the paper.

2. Bearing description

Figure 1 shows the geometry of a circular thrust-bearing separated from the thrust surface by a fluid film thickness. The problem is divided into two regions: region I under the land and region II in the recess. At the outer edges of the bearing under the land, the fluid film thickness is given by $\hat{h}_{\mathrm{I}}$ (carets are henceforth used to denote dimensional quantities). In the recess, the fluid film thickness is given by $\hat{h}_{\mathrm{II}} = \hat{h}_{\mathrm{I}} + \hat{d}$ where $\hat{d}$ is the depth of the recess. The radius of the recess or pocket is denoted by $\hat{R}_p$ while the outer edge of the bearing is $\hat{R}_o$. The (r, θ)-coordinates lie in the plane of the thrust surface with the z-axis perpendicular to that surface. The x-direction is shown in figure 1. For this work, the bearing surfaces are considered to be perfectly flat and the bearing is not tilted, although the moment that induces tilt is evaluated.

The specific application motivating the current study is shown in figure 2. This figure shows one of several bearing/piston assemblies that would be present in an axial piston pump. The bearing is free to pivot at a ball and socket joint where it is connected to a piston which creates the load. The bearing is also submerged in lubricant with viscosity $\hat{\mu}$. The injection pressure provided by a pump (i.e. the pressure at the centre of the bearing) is generally controlled and maintained at a prescribed value $\hat{p}_o$. The corresponding volumetric flow rate of lubricant that is injected into the recess at the bearing centre through a restrictor and a small hole of radius $\hat{\varepsilon}$ is denoted by $\hat{Q}$. The fluid supplied by the pump leaks away from the bearing and creates a pressure distribution between the bearing and the thrust surface. This pressure distribution acts to force the bearing away from the thrust surface, thus creating the load-carrying capacity of the bearing $\hat{W}$. During operation, the thrust surface slides to the left at a prescribed velocity $\hat{U}$. The effect of this sliding surface is to create a skewed pressure profile beneath the bearing which creates a tilting moment $\hat{T}$ on the bearing. The power required to operate the bearing is the sum of

https://doi.org/10.1017/S0022112005003782 Published online by Cambridge University Press

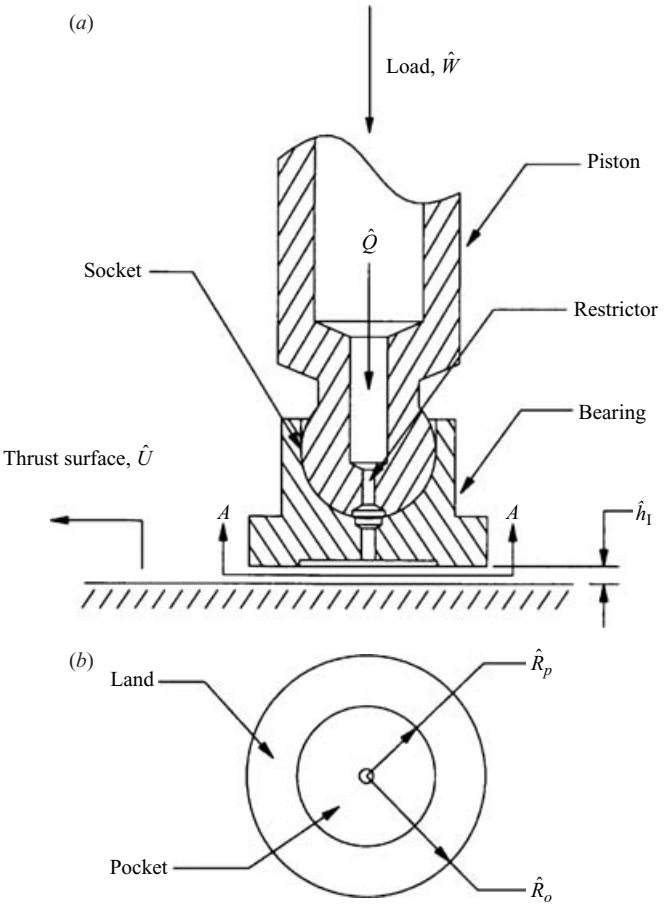


FIGURE 2. (*a*) Bearing piston assembly. (*b*) View *A*–*A*.

the power required for lubricant injection and the power required to overcome the viscous drag associated with the translation.

3. Analysis

A dimensionless formulation is used for easy identification of the important physical factors controlling the physics and to isolate parameters that simply scale the magnitude of the final results. The dimensionless variables used here are defined as

$$p = \frac{\hat{p}}{\hat{\mu}\hat{U}\hat{R}_o/\hat{h}_{\mathrm{I}}^2}, \quad \hat{\boldsymbol{u}} = (u, v) = \frac{\hat{\boldsymbol{u}}}{\hat{U}}, \quad Q = \frac{\hat{Q}}{\hat{U}\hat{h}_{\mathrm{I}}\hat{R}_o}, \quad r = \frac{\hat{r}}{\hat{R}_o}, \quad z = \frac{\hat{z}}{\hat{h}_{\mathrm{I}}}, \tag{1}$$

where p is the pressure and u, v are the velocity components in the plane of the thrust surface, i.e. the (x, y)-plane. With these definitions, the recess radius becomes $R_p = \hat{R}_p/\hat{R}_o$, the recess depth is $d = \hat{d}/\hat{h}_{\mathrm{I}}$, and the dimensionless film thickness in the two regions is $h_{\mathrm{I}} = 1$ and $h_{\mathrm{II}} = \hat{h}_{\mathrm{II}}/\hat{h}_{\mathrm{I}} = 1 + d$. Identifying the characteristic pressure from (1) as $\hat{p}_c = \hat{\mu}\hat{U}\hat{R}_o/\hat{h}_{\mathrm{I}}^2$, note that the dimensionless flow rate can be written in a popular form, $Q = \hat{\mu}\hat{Q}/(\hat{p}_c\hat{h}_{\mathrm{I}}^3)$. Correspondingly, the relationships between force $\hat{W}$

https://doi.org/10.1017/S0022112005003782 Published online by Cambridge University Press

and torque $\hat{T}$ and their dimensionless counterparts (without carets) are

$$\left.\begin{aligned} \hat{W} &= \int_0^{2\pi}\int_0^{\hat{R}_o} \hat{p}\,(\hat{r},\theta)\hat{r}\,\mathrm{d}\hat{r}\,\mathrm{d}\theta = \frac{\hat{\mu}\hat{U}\hat{R}_o^3}{\hat{h}_\mathrm{I}^2}W, \\ \hat{T} &= -\int_0^{2\pi}\int_0^{\hat{R}_o} \hat{x}\,\hat{p}\,(\hat{r},\theta)\hat{r}\,\mathrm{d}\hat{r}\,\mathrm{d}\theta = \frac{\hat{\mu}\hat{U}\hat{R}_o^4}{\hat{h}_\mathrm{I}^2}T. \end{aligned}\right\} \tag{2}$$

Attention is limited to laminar viscous flow valid when the Reynolds number is small and the film thickness or clearance is gradually varying, i.e. the slope of the bearing surface is small. Under these conditions, it is appropriate to use classical lubrication theory. We briefly review this well-known formulation. In this case, the dimensionless flow components in the (x, y)-plane of the thrust surface are introduced and given in the two regions by the expressions (Rowe 1983)

$$\boldsymbol{q}_k = \int_0^{h_k} \boldsymbol{u}(z)\,\mathrm{d}z = -\frac{h_k^3}{12}\nabla p_k - \frac{h_k}{2}\boldsymbol{e}_x \tag{3}$$

where $k = \mathrm{I}$ or II denote the land and recess regions, respectively, $\boldsymbol{e}_x$ is the unit vector in the x-direction, and $\nabla = \boldsymbol{e}_x(\partial/\partial x) + \boldsymbol{e}_y(\partial/\partial y)$ is the two-dimensional gradient operator. The relationship between $\boldsymbol{q}$ and the dimensional flow is $\hat{\boldsymbol{q}} = \hat{U}\hat{h}_\mathrm{I}\boldsymbol{q}$. The second term in (3) is due to the fluid being dragged into the gap by the moving boundary (i.e. Couette flow) and the first term is the Poiseuille flow-like term induced by the pressure field. The pressure distribution $p_k(x, y)$ in the lubricating film is obtained from mass conservation which takes the form

$$\left.\begin{aligned} &\nabla\cdot\boldsymbol{q}_k = 0, \\ &\nabla\cdot\{h_k^3\nabla p_k\} = -6\frac{\mathrm{d}h_k}{\mathrm{d}x}. \end{aligned}\right\} \tag{4}$$

Note that in a small neighbourhood of the rapid transition between the recess and land, the lubrication approximation fails and inertial effects are often important; however, this feature is neglected here. Later we assess when inertial effects might become important by examining the results of numerical simulations of the Navier–Stokes equations that are available in the literature.

Conditions to be satisfied by the solution are: (i) constant pressure at the outer edge of the bearing, $r = 1$, (ii) pressure continuity at the recess edge $r = R_p$, (iii) the flow rate must equal the given injection rate Q, and (iv) the flow rate must be continuous at the recess edge between regions I and II. Therefore

$$p_\mathrm{I} = 0 \quad \text{on} \quad r = 1, \tag{5}$$

$$p_\mathrm{I} = p_\mathrm{II} \quad \text{on} \quad r = R_p, \tag{6}$$

$$\int_0^{2\pi} \boldsymbol{q}_k\cdot\boldsymbol{e}_r r\,\mathrm{d}\theta = Q, \tag{7}$$

$$\boldsymbol{q}_\mathrm{I}\cdot\boldsymbol{e}_r = \boldsymbol{q}_\mathrm{II}\cdot\boldsymbol{e}_r \quad \text{on} \quad r = R_p, \tag{8}$$

where $\boldsymbol{e}_r$ is the unit vector in the radial direction. Note that it is convenient here to treat the injection flow rate Q as known and later deduce the corresponding injection pressure p_o. The above conditions assume the gap is completely filled with lubricant and situations when this may not be satisfied are deduced later from the solution.

Equation (4) for the pressure field reduces to Laplace's equation $\nabla^2 p_k = 0$ in regions $k = \mathrm{I}$ and II, since h_k is constant. Consequently, the solution is a pair of harmonic functions in the two regions that satisfy conditions (5)–(8). The solution must include

https://doi.org/10.1017/S0022112005003782 Published online by Cambridge University Press

a point source term to accommodate the injection condition (7), and it must also include a term to account for the moving boundary, i.e. the second term in (3). The appropriate solutions in the two regions are given in polar coordinates by

$$p_{\mathrm{I}} = -\beta_{\mathrm{I}} \ln r + \left(a_{\mathrm{I}} r + \frac{b_{\mathrm{I}}}{r}\right)\cos\theta \quad \text{for} \quad R_p \leqslant r \leqslant 1, \tag{9}$$

$$p_{\mathrm{II}} = -\beta_{\mathrm{II}} \ln r + \gamma + a_{\mathrm{II}} r \cos\theta \quad \text{for} \quad r \leqslant R_p, \tag{10}$$

where $\beta_{\mathrm{I}}, \beta_{\mathrm{II}}, \gamma, a_{\mathrm{I}}, a_{\mathrm{II}}$ and b_{I} are constants. Vanishing pressure at the bearing edge $r = 1$ (equation (5)), requires $a_{\mathrm{I}} = -b_{\mathrm{I}}$. Pressure continuity at the edge of the recess $r = R_p$ then requires $\gamma = (\beta_{\mathrm{II}} - \beta_{\mathrm{I}}) \ln R_p$ and $a_{\mathrm{II}} = a_{\mathrm{I}}(1 - 1/R_p^2)$ giving

$$p_{\mathrm{I}} = -\beta_{\mathrm{I}} \ln r + a_{\mathrm{I}}\left(r - \frac{1}{r}\right)\cos\theta \quad \text{for} \quad R_p \leqslant r \leqslant 1, \tag{11}$$

$$p_{\mathrm{II}} = -\beta_{\mathrm{II}} \ln \frac{r}{R_p} - \beta_{\mathrm{I}} \ln R_p + a_{\mathrm{I}}\left(1 - \frac{1}{R_p^2}\right) r \cos\theta \quad \text{for} \quad r \leqslant R_p. \tag{12}$$

Continuity of the flow rate in the radial direction at the recess edge, i.e. equation (8), requires

$$\frac{1}{12}\left(\frac{\beta_{\mathrm{I}}}{R_p} - a_{\mathrm{I}}\left(1 + \frac{1}{R_p^2}\right)\cos\theta\right) - \tfrac{1}{2}\cos\theta = \frac{h_{\mathrm{II}}^3}{12}\left(\frac{\beta_{\mathrm{II}}}{R_p} - a_{\mathrm{I}}\left(1 - \frac{1}{R_p^2}\right)\cos\theta\right) - \tfrac{1}{2} h_{\mathrm{II}} \cos\theta. \tag{13}$$

and after using orthogonality

$$\left.\begin{aligned} \beta_{\mathrm{I}} &= \beta_{\mathrm{II}} h_{\mathrm{II}}^3, \\ a_{\mathrm{I}} &= \frac{6(h_{\mathrm{II}} - 1)}{(1 + 1/R_p^2) - h_{\mathrm{II}}^3 (1 - 1/R_p^2)}. \end{aligned}\right\} \tag{14}$$

Lastly, satisfying the prescribed injection rate condition (7) gives

$$\beta_{\mathrm{I}} = \frac{6}{\pi} Q.$$

In summary, the pressure is found as

$$p = \begin{cases} p_{\mathrm{I}} = -\dfrac{6}{\pi} Q \ln r + a_{\mathrm{I}}\left(r - \dfrac{1}{r}\right)\cos\theta \quad \text{for} \quad R_p \leqslant r \leqslant 1, & (15a) \\ p_{\mathrm{II}} = -\dfrac{6}{\pi} Q \left[\dfrac{1}{(1+d)^3} \ln \dfrac{r}{R_p} + \ln R_p\right] + a_{\mathrm{I}}\left(1 - \dfrac{1}{R_p^2}\right) r \cos\theta \ \text{ for } \ r \leqslant R_p, & (15b) \end{cases}$$

where after recalling that $h_{\mathrm{II}} = 1 + d$

$$a_{\mathrm{I}} = \frac{6d}{(1 + 1/R_p^2) - (1+d)^3 (1 - 1/R_p^2)}. \tag{16}$$

Representative pressure distributions predicted by (3) are shown in figure 3 for two representative values of Q; $Q = 1$ and $Q = 0.1$. The case $Q = 0.1$ (figure 3*c*, *d*) corresponds to higher translation speeds. In these two cases, the pressure is nearly linear in the recess and is observed to become negative at the leading edge of the bearing. This would probably trigger cavitation and a resulting change to the pressure field. However, no attempt is made here to analyse the cavitating case, although the

https://doi.org/10.1017/S0022112005003782 Published online by Cambridge University Press

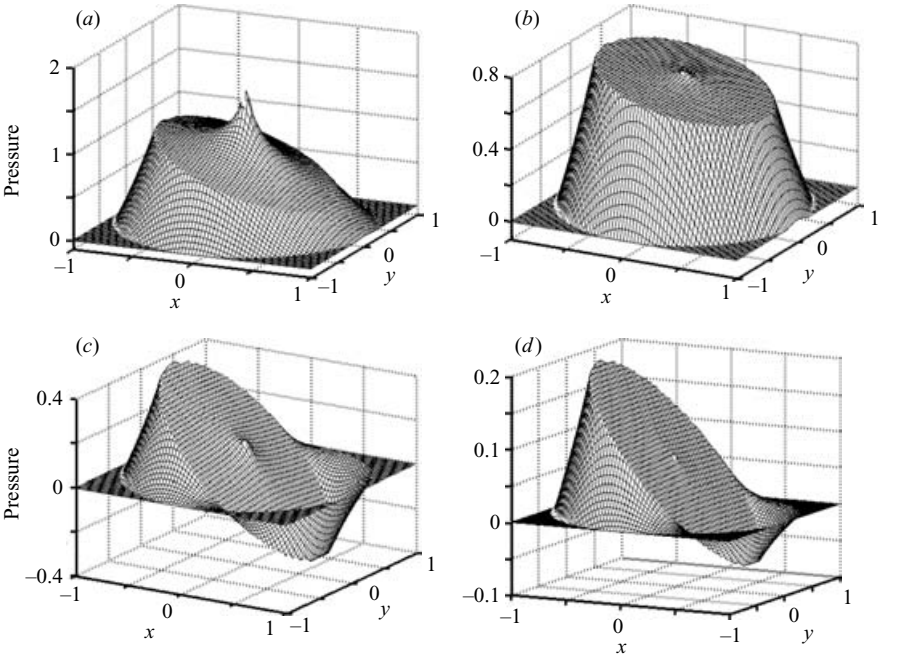


FIGURE 3. Pressure distributions for $R_p = 0.7$ and (*a*) $Q = 1$, $d = 1$, (*b*) $Q = 1$, $d = 4$, (*c*) $Q = 0.1$, $d = 1$, (*d*) $Q = 0.1$, $d = 4$. $\varepsilon = 0.02$.

model can predict incipient conditions for cavitation. At lower speeds, when $Q = 1$ and the recess is fairly deep with $d = 4$ (figure 3*b*), the pressure in the recess is nearly constant. As $d \to \infty$ for Q constant, the well-known result of a nearly constant pressure in the recess is easily obtained from (15) and (16). However, contrasting the two deep cases when $d = 4$, (figure 3*b*, *d*) it is clear that as translation speed increases (and Q decreases), the linear variation of pressure in the recess will manifest itself (figure 3*d*). Also note the source-like term at the origin when the injection rate is significant ($Q = 1$) and the recess is shallow, $d = 1$ (figure 3*a*). The linear pressure variation in the recess is due to the translation or Couette flow effect and the contrast between Couette-dominated and injection-dominated flow has been discussed for the two-dimensional case on several occasions (e.g. Braun & Dzodzo, 1995).

In practice, it is more common to prescribe the injection pressure and not the injection flow rate. Therefore we define the injection pressure p_o as the average pressure over the circumference of the small injection hole of radius $r = \varepsilon$. This yields, from (15*b*), the relationship between injection rate and injection pressure

$$Q = \frac{\pi p_o}{6\{(1+d)^{-3}\ln(R_p/\varepsilon) - \ln R_p\}}. \tag{17}$$

Naturally, there is a pressure drop through the orifice where the lubricant is injected. Therefore a separate model of the supply system must be constructed if we want to evaluate the required upstream source pressure. Figure 4 shows the dimensionless flow rate normalized by the pressure term p_o. It is noteworthy that leakage rates can become large for deep and wide recesses; later, it will be apparent that this trend dramatically affects the power consumed.

https://doi.org/10.1017/S0022112005003782 Published online by Cambridge University Press

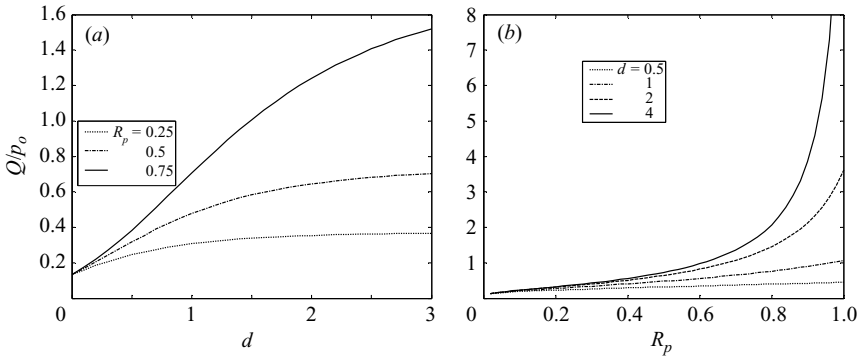


FIGURE 4. Dimensionless flow rate Q divided by p_o (see equation (17)) (a) versus d and (b) versus R_p using $\varepsilon = 0.02$.

The dimensional result corresponding to (17) is

$$\hat{Q} = \frac{\hat{h}_{\mathrm{I}}^3 \hat{p}_o}{\hat{\mu}} \frac{\pi}{6\{(1+d)^{-3}\ln(R_p/\varepsilon) - \ln R_p\}},$$

which reduces to the well-known deep-recess result (Rowe 1983; Bassani & Piccigallo 1992)

$$\hat{Q} = \frac{\hat{h}_{\mathrm{I}}^3 \hat{p}_o}{\hat{\mu}} \frac{\pi}{6\ln(1/R_p)}.$$

Note also that $\hat{p}_o/\hat{Q}$ is sometimes referred to as the 'hydraulic resistance'.

3.1. *Lift and tilting moment*

The dimensionless supporting lift force or load-carrying capacity of the bearing is given by

$$W = \int_0^{2\pi}\int_0^1 p(r,\theta) r \,\mathrm{d}\theta \,\mathrm{d}r = \int_0^{2\pi}\left\{\int_0^{R_p} p_{\mathrm{II}} r \,\mathrm{d}r + \int_{R_p}^1 p_{\mathrm{I}} r \,\mathrm{d}r\right\}\mathrm{d}\theta$$
$$= 3Q\left\{1 - R_p^2\left[1-(1+d)^{-3}\right]\right\}. \tag{18}$$

Note that the force is due exclusively to the injection flow, but is independent of the pressure field induced by the bearing translation. Furthermore, (17) can be conveniently used in (18) to eliminate the injection flow rate in preference to the injection pressure to yield

$$W = \frac{\pi p_o}{2} \frac{1 - R_p^2[1-(1+d)^{-3}]}{(1+d)^{-3}\ln(R_p/\varepsilon) - \ln R_p}. \tag{19}$$

The corresponding dimensional result follows from (2) and (19) as

$$\hat{W} = \frac{\hat{\mu}\hat{U}\hat{R}_o^3}{\hat{h}_{\mathrm{I}}^2} W = \hat{p}_o \hat{R}_o^2 \frac{\pi}{2} \frac{1 - R_p^2[1-(1+d)^{-3}]}{(1+d)^{-3}\ln(R_p/\varepsilon) - \ln R_p}. \tag{20}$$

For the deep-recess case when the pressure in the recess is nearly constant, the well-known result emerges (Rowe 1983; Bassani & Piccigallo 1992)

$$\hat{W} = \hat{p}_o \hat{R}_o^2 \frac{\pi}{2} \frac{R_p^2 - 1}{\ln R_p}. \tag{21}$$

https://doi.org/10.1017/S0022112005003782 Published online by Cambridge University Press

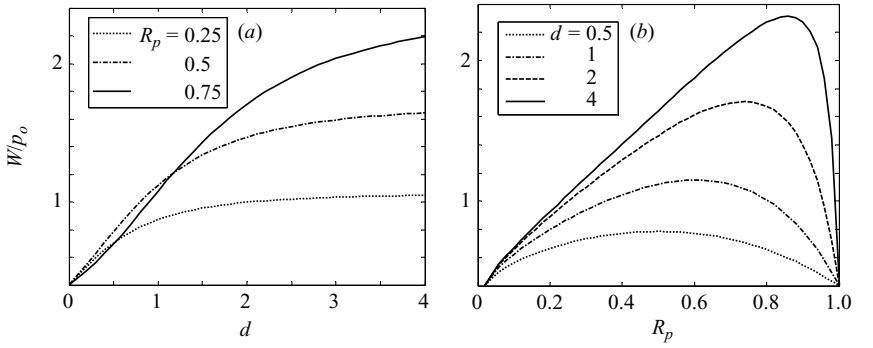


FIGURE 5. Dimensionless load divided by p_o (see equation (19)) (*a*) versus d and (*b*) versus R_p.

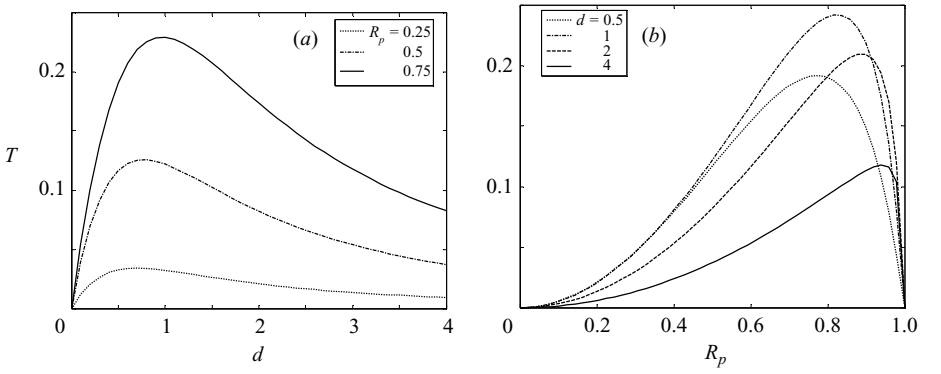


FIGURE 6. Dimensionless tilting moment (equation (22)) (*a*) versus d and (*b*) versus R_p.

The load W/p_o obtained from (19) is shown in figure 5. The load reaches its maximum when the depth of the recess is only a few times that of the film under the lands. The maximum load-carrying capacity also shifts from about $R_p = 0.5$ for very shallow recesses to a value near $R_p = 0.86$ as the recess increases in depth to $d = 4$. As the recess width increases further, the load capacity suddenly drops to a limiting value of 0.4.

Since circular thrust bearings are often mounted using a ball-and-socket fixture (figure 2), bearing tilt can play an important role in wear. Although translation has no effect on the load-carrying capacity of the bearing, it is solely responsible for the tendency for the bearing to tilt forward about an axis perpendicular to the direction of travel, i.e. the y-axis. Furthermore, the moment that induces this tilt is independent of injection pressure or flow rate. Computing the moment gives

$$T = \int_0^{2\pi}\int_0^1 -xp(r,\theta)r\,\mathrm{d}\theta\,\mathrm{d}r = \int_0^{2\pi}\left\{-\int_0^{R_p} p_{\mathrm{II}}r^2\,\mathrm{d}r - \int_{R_p}^1 p_{\mathrm{I}}r^2\,\mathrm{d}r\right\}\cos\theta\,\mathrm{d}\theta$$

$$= \frac{\pi a_{\mathrm{I}}}{4}\left(1-R_p^2\right) = \frac{3\pi}{2}\left(\frac{d\left(1-R_p^2\right)}{\left(1+1/R_p^2\right)-(1+d)^3\left(1-1/R_p^2\right)}\right). \tag{22}$$

For deep pockets, the tilting moment clearly vanishes, demonstrating one inherent advantage of deep-recess designs (also see figure 6*a*). However, a disadvantage observed earlier is the poor leakage efficiency. The corresponding dimensional tilting

https://doi.org/10.1017/S0022112005003782 Published online by Cambridge University Press

moment is

$$\hat{T} = \frac{\hat{\mu}\hat{U}\hat{R}_o^4}{\hat{h}_\mathrm{I}^2}\frac{3\pi}{2}\left(\frac{d\left(1-R_p^2\right)}{\left(1+1/R_p^2\right)-(1+d)^3\left(1-1/R_p^2\right)}\right). \tag{23}$$

The behaviour of the tilting moment T is plotted versus d in figure 6(a) and versus R_p in figure 6(b). When d is between 0.5 and 1.0, the tilting moment reaches a maximum. The moment asymptotes to zero as the recess becomes deep and has decreased from its maximum value by about half when it reaches $d=4$. The moment also has a maximum for recesses with relatively large radii and this maximum occurs for values of R_p greater than about 0.75 (figure 6b). The maximum value when $d=4$ occurs for very narrow lands when $R_p \approx 0.95$.

3.2. *Power*

The power $\hat{E}$ required to sustain the lubricant injection and to overcome the viscous drag associated with bearing translation is

$$\hat{E} = \hat{p}_o\hat{Q} + \hat{U}\int_0^{2\pi}\int_0^{\hat{R}_o}\hat{\tau}_{xz}(\hat{z}=0)\hat{r}\,\mathrm{d}\hat{r}\,\mathrm{d}\theta, \tag{24}$$

where $\hat{\tau}_{xz}$ is the viscous shear stress given in each region ($k=$ I or II) by

$$\hat{\tau}_{xz}^{(k)} = \hat{\mu}\frac{\partial\hat{u}}{\partial\hat{z}} = \frac{\partial}{\partial\hat{z}}\left[\frac{1}{2}\frac{\partial\hat{p}}{\partial\hat{x}}(\hat{z}^2-\hat{h}_k\hat{z}) - \hat{\mu}\hat{U}\left(1-\frac{\hat{z}}{\hat{h}_k}\right)\right]$$

$$= \frac{1}{2}\frac{\partial\hat{p}}{\partial\hat{x}}(2\hat{z}-\hat{h}_k) + \frac{\hat{\mu}\hat{U}}{\hat{h}_k}, \tag{25a}$$

$$\hat{\tau}_{xz}^{(k)}(\hat{z}=0) = -\frac{1}{2}\frac{\partial\hat{p}}{\partial\hat{x}}\hat{h}_k + \frac{\hat{\mu}\hat{U}}{\hat{h}_k}. \tag{25b}$$

Note that the second term in (25a) is the viscous shear stress due to the motion of the thrust surface and the first term involving the pressure gradient is the shear stress associated with the recirculation created by the recess. Using (25), the power is found to be

$$\hat{E} = \pi\left\{\frac{\hat{p}_o^2\hat{h}_\mathrm{I}^3}{6\hat{\mu}}\left[\frac{1}{(1+d)^{-3}\ln(R_p/\varepsilon)-\ln R_p}\right] + \frac{\hat{\mu}\hat{U}^2\hat{R}_o^2}{\hat{h}_\mathrm{I}}\left[\frac{R_p^2}{1+d}+1-R_p^2\right]\right\}$$

$$= \frac{\hat{\mu}\hat{U}^2\hat{R}_o^2}{\hat{h}_\mathrm{I}}\pi\left\{p_o^2\left[\frac{1}{(1+d)^{-3}\ln(R_p/\varepsilon)-\ln R_p}\right] + \left[\frac{R_p^2}{1+d}+1-R_p^2\right]\right\}. \tag{26}$$

A suitable dimensionless power for examining trends is $\dot{E} = \hat{E}/(\hat{\mu}\hat{U}^2\hat{R}_o^2/\hat{h}_\mathrm{I})$. Notice that the first term in (26) is due to leakage and is proportional to the square of the dimensionless pressure. The second term is the drag contribution.

The term involving the pressure gradient in (25), which can be identified with the recirculating flow, makes no net contribution to the drag and therefore the power. The viscous drag created by recirculation in the recess is exactly offset by a thrust created under the lands by the large pressure gradient there (see figure 3). Therefore, the net drag is only due to the viscous stress associated with the Couette flow in each region. This is most easily appreciated by evaluating the corresponding two-dimensional problem (unpublished work). In that case, (25) is still valid but the integration of the shear stress in (24) is only with respect to $\hat{x}$ from, say, $-\hat{L}$ to $\hat{L}$. Since the gap is constant and the pressure is continuous and begins and ends at the same value (i.e.

https://doi.org/10.1017/S0022112005003782 Published online by Cambridge University Press

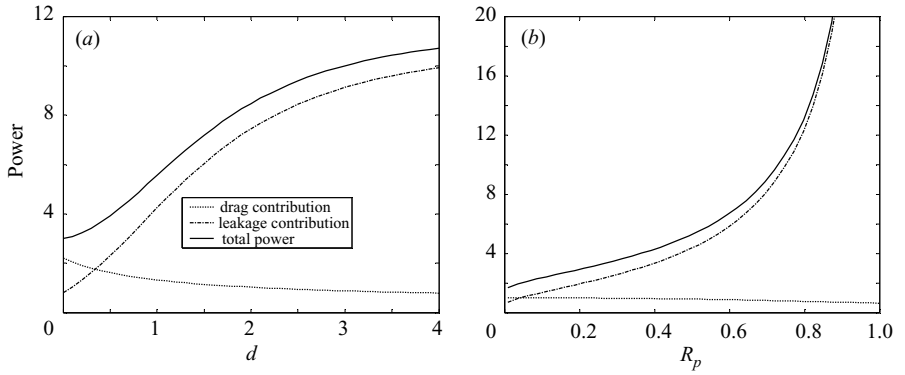


FIGURE 7. Dimensionless power (a) versus d for $R_p = 0.75$ and $p_o = 1$; (b) versus R_p for $d = 4$ and $p_o = 1$. $\varepsilon = 0.02$ in both.

p vanishes), the net contribution from the integration of $\mathrm{d}p/\mathrm{d}x$ clearly vanishes. This result is apparently only true when the gap is constant. On occasion, authors have accounted for the recirculating flow in the recess and overlooked the corresponding flow under the lands, thereby leading to an erroneous result. Reflecting on the basic physics, it becomes evident that the drag could not be greater than that generated by the translating plate and induced Couette flow (at least within the scope of the lubrication approximation used here).

The dimensionless pressure (recall (1)) for a 1 in. diameter bearing operating at 4000 p.s.i. (27.6 MPa), translating at $10\,\mathrm{m\,s^{-1}}$ in 30 W oil (80 °C) with a clearance $\hat{h}_\mathrm{I} = 10\,\mu\mathrm{m}$ is approximately $p_o \approx 1$. Using this value, the dimensionless power is plotted in figure 7 versus dimensionless recess depth d and radius R_p. Since it can be convenient to examine the behaviour relative to the width of the lands, recall that the dimensionless land width is $1 - R_p$. Therefore, wide lands correspond to $R_p = 0$ and $R_p \to 1$ for narrow lands. Figure 7 shows the two contributions to the power; the power consumed by viscous drag and the power used to inject the lubricant. The contribution from the drag is nearly constant and generally a smaller contribution to the power than the leakage contribution. The net power is nearly constant for $d > 4$ and rises very rapidly for narrow lands when $R_p > 0.7$. The rapid rise as R_p exceeds 0.7 is due to the low resistance to leakage provided by the relatively narrow lands causing a large flow rate of lubricant from the bearing.

It is also useful in design to consider the power consumed for a fixed load-carrying capacity. To accomplish this, the pressure $\hat{p}_o$ can be eliminated in (26) in preference for the load $\hat{W}$ using (20). Since the pressure only appears in the power term associated with lubricant injection, i.e. the leakage term (first term in (26)), we express this part of the power as

$$\hat{\dot{E}}_{leakage} = \tfrac{2}{3}\pi \frac{\hat{W}^2 \hat{h}_\mathrm{I}^3}{\hat{\mu}\hat{R}_o^4} \left[\frac{(1+d)^{-3}\ln(R_p/\varepsilon) - \ln R_p}{\left[1 - R_p^2\{1-(1+d)^{-3}\}\right]^2} \right] = \frac{\hat{W}^2 \hat{h}_\mathrm{I}^3}{\hat{\mu}\hat{R}_o^4} \dot{E}_{leakage}. \tag{27}$$

The dimensionless power to support the lubricant injection $\dot{E}_{leakage}$ is shown versus R_p in figure 8 for several values of the recess depth d. There is a fairly wide range from about $R_p = 0.25$ to 0.75 when the leakage power maintains a relatively low value. The absolute minimum shifts towards larger values of R_p as the recess becomes deep, and very shallow recesses generally require about 25 % to 30 % more power in this minimum power region where the curves are fairly flat. Recall that the power to

https://doi.org/10.1017/S0022112005003782 Published online by Cambridge University Press

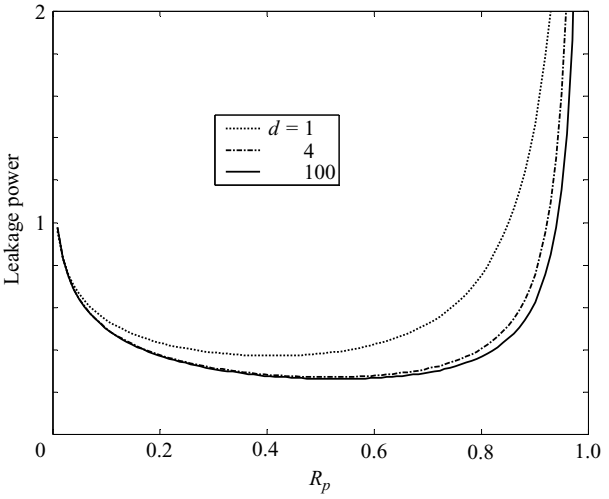


FIGURE 8. Dimensionless leakage power $\dot{E}_{leakage}$ versus R_p for several values of d ($\varepsilon = 0.02$).

overcome viscous drag, which varies only slightly with R_p must be added to yield the total power.

4. Flow pattern

We can look at the flow pattern or streamlines under the bearing in the plane of the thrust surface by defining the streamfunction ψ in terms of the flow components in the radial and azimuthal directions: $q_r = (1/r)(\partial\psi/\partial\theta)$, $q_\theta = -\partial\psi/\partial r$. These yield the following streamfunction

$$\psi = \begin{cases} -\left[\dfrac{h_{\rm II}}{2} + \dfrac{a_{\rm I} h_{\rm II}^3}{12}\left(1 - \dfrac{1}{R_p^2}\right)\right] r\sin\theta + \dfrac{Q}{2\pi}\theta & \text{for} \quad r < R_p, \\ -\left[\tfrac{1}{2} + \dfrac{a_{\rm I}}{12}\left(1 + \dfrac{1}{r^2}\right)\right] r\sin\theta + \dfrac{Q}{2\pi}\theta & \text{for} \quad R_p \leqslant r \leqslant 1, \end{cases} \tag{28}$$

where $a_{\rm I}$ is given in (16). Several examples of the predicted streamlines are shown in figure 9 where the flow of fluid is from right to left. The solid circle is the edge of the bearing and the dotted circle is the edge of the recess. The long and short dashed line is the stagnation streamline which is the demarcation between the injected lubricant and the upstream flow. The critical injection rate above which injected lubricant wets the entire surface under the bearing can be found by evaluating Q when the stagnation point is located at the edge of the bearing, i.e. $q_r(r = 1,\ \theta = 0) = 0$. This yields $Q_{crit} = \pi(1 + a_{\rm I}/3)$ and for values of Q larger than this value, the injected lubricant will flood the entire region under the bearing. Exceeding this critical value might be beneficial since it might preclude entraining any debris in the free stream from being trapped under the bearing. Debris can sometimes adversely impact wear. In figure 9, the critical values are $Q_{crit} = 3.358$ when $d = 1$ and $R_p = 0.5$ and $Q_{crit} = 3.694$ when $d = 4$ and $R_p = 0.7$. Therefore the fully wetted condition is being approached in the right-hand figures where $Q = 3$. Using (17), the corresponding critical pressure can be readily obtained. The stagnation streamline also suggests that, if the injection rate is not sufficiently large and the bearing is not operating in a flooded environment, a portion of the thrust surface under the bearing might be dry since no incoming fluid

https://doi.org/10.1017/S0022112005003782 Published online by Cambridge University Press

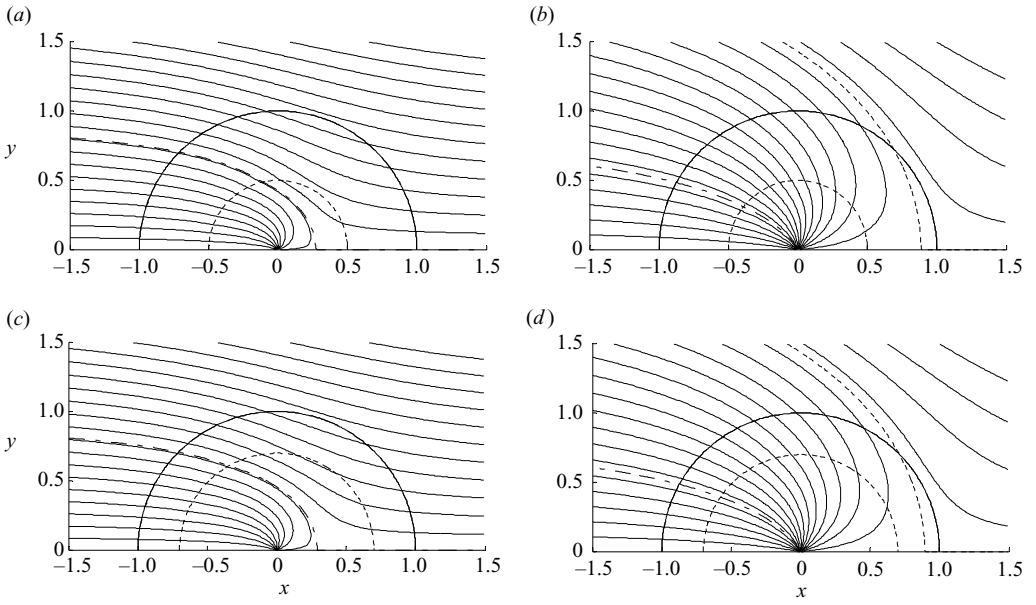


FIGURE 9. Streamlines (flow is from right to left): (*a*) $R_p = 0.5$, $d = 1$ and $Q = 1$, (*b*) $R_p = 0.5$, $d = 1$ and $Q = 3$, (*c*) $R_p = 0.7$, $d = 4$ and $Q = 1$, and (*d*) $R_p = 0.7$, $d = 4$ and $Q = 3$.

would be present. This is very apparent in the figures on the left-hand side where the separating streamline emanates from within the recess. This stagnation streamline is only suggestive of a partial dry-out condition, since a separate free-stream analysis would be required to accurately evaluate this case.

5. Limitation due to inertial effects

It was noted earlier that the lubrication approximation neglects inertial effects and therefore it is useful to explore the limits beyond which the current predictions would be of little value. Although experiments are not available for this purpose, numerical simulations of the Navier–Stokes equations are of considerable use in shedding light on this issue. Unfortunately, in making comparisons there are significant differences between cases available in the literature and that considered here. One limitation is the fact that numerical simulations have focused on two-dimensional journal bearings and have not investigated circular thrust bearings. A few three-dimensional simulations of rectangular journal bearings are available, but the fundamental difference in geometry allows only qualitative comparisons. A second issue is that the present study provides closed-form expressions of value in engineering design such as load-carrying capacity, tilting moment, leakage and power consumption. The computational literature on the other hand focuses on details of the pressure distributions and flow patterns. In spite of these differences, the numerical results provide some estimates and guidelines for application of the current work. Several of the inertial flow characteristics of interest are: the pressure peaks often associated with the Rayleigh step, inertia-induced pressure drops that occur, and flow pattern characteristics that are attributable to inertia. Effects on the pressure are of obvious potential importance to force and torque results.

https://doi.org/10.1017/S0022112005003782 Published online by Cambridge University Press

A good place to start is the Navier–Stokes simulation conducted by Braun & Dzodzo (1995) for a two-dimensional journal bearing. Their study presents detailed results for the pressure distribution and streamlines in the two basic flow regimes: a flow dominated by the Couette effects and a case dominated by the flow due to lubricant injection. Six different clearances under the land were considered corresponding to $d = \hat{d}/\hat{h}_1 = 1$, 2, 5, 20, 40 and 100. In the present analysis, the transition from Couette-dominated to injection-dominated flow occurs as Q increases (or correspondingly p_o), but unfortunately Q is not available because of the fundamental difference between two-dimensional and circular bearing cases. Note also that in contrast to Braun & Dzodzo, the discussion here uses a Reynolds number based on the recess depth $\hat{d}$, i.e. $Re = \rho \hat{U} \hat{d}/\mu$.

Much can be garnered by examining the pressure distributions and the presence or absence of the inertial flow characteristics in Braun & Dzodzo's results. Specifically, on examining the pressure fields in their figures 5 and 6, it is apparent that when the recess is relatively shallow ($d = 1$, 2, 5) and $Re = 10$ or $Re = 80$, inertial flow features are minor. Inertial flow characteristics are also minor when $Re = 200$ and the recess is deep ($d = 20$, 40, 100). In these cases, inertial peaks associated with the Rayleigh step are absent and modest inertial pressure drops are present near the transition from recess to land. A crude estimate indicates that neglecting these inertial features would lead to an error of less than 5 %. In the case when $Re = 1600$ and the recess is deep ($d = 20$, 40, 100), the pressure is nearly constant in the recess and a pressure peak due to the Rayleigh step is apparent. However, the magnitude of the peak is modest and has a small spatial extent such that its net effect on the force will be small. The width of the pressure peak is observed to be about 5–10 times the film thickness under the land.

The Rayleigh step effect will probably have the greatest effect on the tilting moment since this pressure peak occurs at the downstream transition to the land and therefore it has a sizeable moment arm. Even small tilting moments are relevant since circular thrust bearings are often mounted by ball joints that are lubricated by the same high-pressure source as the injection port (figure 2). The numerical simulations show that for $Re \geqslant 1600$ and deep pockets, the Rayleigh step effect is often present and the current predictions for tilting moment would be questionable.

Helene, Arghir & Frene (2003) also examined laminar flow in a two-dimensional journal bearing, but extended the analysis to include turbulent flows using a classical k–ε model of turbulence. In the laminar regime, they obtain qualitative agreement with the results of Braun & Dzodzo (1995). Reynolds numbers covered the range from 0 to 800 and six values of d were considered between 4 and 152. For all recess depths and $Re \leqslant 100$, Helene *et al.* found that the pressure in the recess is nearly constant and appears to be linearly decreasing under the lands, as would be predicted by lubrication theory. When $Re = 400$ and $d = 4$, a slight pressure variation occurs in the recess that is similar to the linear variation associated with the Couette dominated flow. At $Re = 400$ and $d \geqslant 8$, a slight Rayleigh step effect is apparent and, although it would have negligible effect on the force, it would begin to influence the torque. However, when the Reynolds number increases to 800, a sizeable Rayleigh step effect is clearly present, indicating that the present results would be suspect. Also note that Braun, Choy & Zhou (1993) found very similar results in their numerical simulations for Re between 100 and 400.

Although no attempt is made to compare the results to the turbulent-flow case examined by Helene *et al.* it is appropriate to consider the limits to laminar flow. Unfortunately, an analysis of flow stability in the current configuration does not

https://doi.org/10.1017/S0022112005003782 Published online by Cambridge University Press

appear to be available; however, it is well known that plane Poiseuille flow is stable up to a Reynolds number of 5772 and that it is generally stabilized by the superposition of a Couette flow. More conservatively, Bassani & Piccigallo (1992) place the safe upper limit for assuming laminar flow in bearings at $Re = 1000$.

A three-dimensional Navier–Stokes simulation for a hydrostatic journal bearing with a rectangular pocket was conducted by Braun & Dzodzo (1997). Laminar flow was considered with $Re = 72$ and $d = 4.5$. Although explicit comparison cannot be made to the present case, the three-dimensional pressure profiles are reminiscent of those found here with a nearly linear pressure variation in the recess and a rapid decrease under the land. A very small Rayleigh step pressure rise is observed, but this would have negligible effect on the load-carrying capacity or tilting moment.

In summary, the qualitative comparison to two-dimensional numerical results and the limited number of three-dimensional results suggests that the current model should reasonably predict force for $Re \leqslant 400$. However, tilting moment predictions would become questionable as the Reynolds number reaches 400 and the Rayleigh step effect can be anticipated. It can also be expected that the current power predictions would be useful for Re up to 400. The current results show that power requirements are dominated by the leakage flow contribution and the leakage flow rate is largely dictated by the flow restriction under the land. Inertia will have a more significant effect on the recirculating flow in the recess and therefore it will have a greater influence on the shear drag.

6. Conclusion

This paper has determined closed-form expressions for several quantities of engineering interest regarding translating circular thrust bearings. Several trends have been explored, including load-carrying capacity, tilting moment, leakage rate and power consumption. The significance of sliding speed may be assessed based upon the examination of the parameter $Q = \hat{Q}/\hat{U}\hat{h}_1\hat{R}_o$. When Q is small, sliding speed effects begin to dominate. The sliding speed tends to skew the pressure distribution between the bearing and the thrust surface and it is the source of the tilting moment. The tilting moment is independent of the rate of lubricant injection or injection pressure. Wide pockets generally exhibit the greatest tilting moment for bearings of similar size, operating at the same speed and using the same lubricant. A maximum tilting moment is observed at a critical value of the recess radius (figure 6*b*). Therefore, this design condition should be avoided if one desires to minimize the tilting effect.

Bearings operating at higher speed, i.e. low values of Q, can experience dry-out, if they are not working in a flooded environment. Furthermore, for high-velocity operation, the skewed pressure distribution can also cause cavitation at the leading edge of the bearing. In addition, the results show that designing a circular thrust bearing with a shallow recess exhibits advantages and disadvantages. The advantage of using this design is that it tends to require less power to operate, without sacrificing significant load-carrying capacity. A disadvantage of a shallow recess design is that the tilting moment is generally largest. Large recesses with deep pockets exhibit the largest load-carrying capacity for bearings of similar size and having the same injection pressure. As the recess depth increases, the maximum load-carrying capacity shifts to increasing values of the recess radius.

Bearing leakage increases rapidly for deep recesses when $R_p > 0.7$, i.e. as the land becomes narrow. For example, when $d = 4$ the leakage increases by more than 50 % as the recess increases in radius from $R_p = 0.7$ to $R_p = 0.8$. Furthermore, the

https://doi.org/10.1017/S0022112005003782 Published online by Cambridge University Press

corresponding power required to operate a bearing is often dominated by the leakage effect and the power increases rapidly when $R_p > 0.7$.

The authors would like to thank the National Science Foundation (DMI 0100279) and Caterpillar, Inc. for their support of this work. The authors would also like to thank Professor Cherukuri, Professor Kim and Mr Feng for many interesting discussions concerning thrust bearings.

REFERENCES

Bassani, R. & Piccigallo, B. 1992 *Hydrostatic Lubrication*. Elsevier.

van Beek, A. 2004 *Machine Lifetime Performance and Reliability*. Tribos (ISBN: 90 3700 208 0).

van Beek, A. & Ostayen, R. 1997 Analytical solution for tilted hydrostatic multi-pad thrust bearings of infinite length. *Tribology Intl* **30**, 33–39.

van Beek, A. & Segal, A. 1997 Numerical solution for tilted hydrostatic multi-pad thrust bearing of finite length. *Tribology Intl* **30**, 41–46.

Braun, M. J., Choy, F. K. & Zhou, Y. M. 1993 The effects of a hydrostatic pocket aspect ratio, supply orifice position, and attack angle on steady-state patterns, pressure, and shear characteristics. *J. Tribology* **115**, 678–685.

Braun, M. J. & Dzodzo, M. 1995 Effects of the feedline and the hydrostatic pocket depth on the flow pattern and pressure distribution. *J. Tribology* **117**, 224–233.

Braun, M. J. & Dzodzo, M. 1997 Three-dimensional flow and pressure patterns in a hydrostatic journal bearing pocket. *J. Tribology* **119**, 711–719.

Dadouche, A., Fillon, M. & Bligoud, J. 2000 Experiments on thermal effects in a hydrodynamics thrust bearing. *Tribology Intl* **33**, 167–174.

Davies, P. 1974 Investigation of an all-metallic flexible hydrostatic thrust bearing. *ASLE Trans.* **17**, 117–126.

Dowson, D. & Taylor, C. 1967 Elastohydrostatic lubrication of circular plate thrust bearings. *J. Lubr. Tech.* July, 237–244.

Hamrock, B. 1994 *Fundamentals of Fluid Film Lubrication*. McGraw-Hill.

Helene, M., Arghir, M. & Frene, J. 2003 Numerical study of the pressure pattern in a two-dimensional hybrid journal bearing recess, laminar, and turbulent flow results. *J. Tribology* **125**, 283–290.

Iboshi, N. & Yamaguchi, A. 1982 Characteristics of a slipper bearing for swash plate type axial piston pumps and motors – 1st report: Theoretical analysis. *Bull. JSME* **25**, 1921–1930.

Iboshi, N. & Yamaguchi, A. 1986 Characteristics of a slipper bearing for swash plate type axial piston pumps and motors – 4th report: Effects of surface roughness. *Bull. JSME* **29**, 2539–2546.

Ivantysyn, J. 1999 Sliding bearing with self-adjusted load bearing capacity. United States Patent No. 5,983,781. Assignee: Sauer Inc., Ames, Iowa.

Kazama, T. & Yamaguchi, A. 1993 Optimum design of bearing and seal parts for hydraulic equipment. *Wear* **161**, 161–171.

O'Donoghue, J. & Hooke, C. 1969 Design of inherently stable hydrostatic bearings. *Proc. Instn, Mech. Engrs* **183**, 172–176.

Osman, T., Dorid, M., Safar, Z. & Mokhtar, M. 1996 Experimental assessment of hydrostatic thrust bearing performance. *Tribology Intl* **29**, 233–239.

Rowe, W. B. 1983 *Hydrostatic and Hybrid Bearing Design*. Butterworths.

San Andrés, L. 2000 Bulk-flow analysis of hydrid thrust bearings for process fluid applications. *J. Tribology* **122**, 170–180.

Shinkle, J. & Hornung, K. 1965 Frictional characteristics of liquid hydrostatic journal bearings. *Trans ASME J. Basic Engng* March, 163–169.

Storteig, E. & White, M. 1999 Dynamic characteristics of hydrodynamically lubricated fixed-pad thrust bearings. Wear **232**, 250–255.

Szeri, A. Z. 1998 *Fluid Film Lubrication*. Cambridge University Press.

Wang, X., Zhang, Z. & Zhang, G. 1999 Improving the performance of spring-supported thrust bearing by controlling its deformations. *Tribology Intl* **32**, 713–720.

https://doi.org/10.1017/S0022112005003782 Published online by Cambridge University Press